Surface phonon dispersion of $ZrB_2(0001)$ and $NbB_2(0001)$

Takashi Aizawa, Wataru Hayami, and Shigeki Otani
Advanced Materials Laboratory, National Institute for Materials Science, 1-1 Namiki, Tsukuba, Ibaraki 305-0044, Japan
(Received 26 July 2001; published 19 December 2001)

Surface phonon-dispersion relations for $ZrB_2(0001)$ and $NbB_2(0001)$ are measured by high-resolution electron-energy-loss spectroscopy. In addition to the acoustic surface modes, phonon modes of the graphitelike boron sheet are observed. The boron phonon modes are more complex and softer on $NbB_2(0001)$ than on $ZrB_2(0001)$. This is consistent with the metal- and boron-layer termination of $ZrB_2(0001)$ and $NbB_2(0001)$ surfaces, respectively. The phonon dispersion is analyzed by a force-constant model. By a simple force-constant model, the boron phonon modes are reproduced fairly well. The obtained force constants show that the B-B bond strength is comparable to the B-M bond. The B-B bond in NbB_2 is stronger than in ZrB_2.

DOI: 10.1103/PhysRevB.65.024303 PACS number(s): 68.35.Ja, 63.20.Dj, 68.35.Bs

I. INTRODUCTION

Transition-metal diboride (MB_2) has a hexagonal layered crystal structure, or an AlB_2-type, in which honeycomb boron sheets and close-packed metal layers stack alternately. While they are metallic in the electronic structure, strong covalent bonds give them high melting points and a high degree of hardness suitable for various applications to, for example, an electron emitter, a catalyst, a protective coating, and so on. For these applications, basic knowledge of the surface is essential.

Very recently, superconductivity of MgB_2 at exceptionally high temperature (39 K) has been found.[1] MgB_2 also has the AlB_2-type crystal structure. The isotope effect shows that the phonon of the boron lattice must play an important role in the superconductivity.[2] But unfortunately, no phonon-dispersion data is available either for the simple-metal diboride or for the transition-metal diboride.

As for surface structures of MB_2, $HfB_2(0001)$ (Ref. 3) and $TaB_2(0001)$ (Ref. 4) surfaces have been investigated by impact-collision ion scattering spectroscopy (ICISS). It was revealed that the $HfB_2(0001)$ surface is terminated with the metal layer while the $TaB_2(0001)$ surface consists of the graphitelike boron layer. This tendency was well explained by the total-energy calculation with use of the first-principles pseudopotential method.[5]

Generally speaking, the surface phonon can be different from the bulk one, because of bond breaking and the following relaxation at the surface. Therefore, it is difficult to interpret the surface phonon without the bulk phonon data. However, in a layered material like graphite, the large unisotropy may reduce the difference between the bulk phonon and the surface phonon.[6] As shown in the following sections, the interlayer interaction in MB_2 is not so small, as in graphite, that the surface effect cannot be neglected. But a large mass difference between the metal and the boron allows the high-energy phonon to be localized in the boron layer, and makes the interpretation of the dispersion easier.

In this paper, the $ZrB_2(0001)$ and $NbB_2(0001)$ surface phonon-dispersion data are measured by high-resolution electron-energy-loss spectroscopy (HREELS). The dispersion data are interpreted by using force-constant model calculations.

II. EXPERIMENT

The experiment was done in an ultrahigh-vacuum chamber made of an Ni-Fe alloy of high permeability (PC permalloy). The residual magnetic field at the sample position was less than 10^{-6} T. The chamber is equipped with a HREELS spectrometer (VSI Delta0.5), low-energy electron-diffraction (LEED) optics to determine the sample azimuth, and a sample preparation chamber. The main chamber is evacuated by a 500 l/s turbomolecular pump, a Ti getter pump, and a nonevaporate getter pump (SAES B-1300), achieving the base pressure of 2×10^{-9} Pa. The working pressure during the HREELS measurement was $3.5–4.0\times10^{-9}$ Pa.

The HREELS spectrometer is the so-called "Ibach type,"[7] which consists of a double-pass cylindrical-deflector electron monochromator and a single-pass energy analyzer. Electron lenses are placed at each an entrance and exit of the monochromator and the analyzer. The potential of the electrodes is supplied by a computer-controlled precise digital-to-analog converter. The best resolution of the system at the straight-through mode is 0.4 meV. In this experiment, the energy resolution of ~2 meV was applied in order to get more current and to improve the signal-to-noise ratio in the off-specular measurements.

The stainless-steel preparation chamber is equipped with a reflection high-energy electron-diffraction (RHEED) system, a cylindrical mirror analyzer for Auger electron spectroscopy (AES), a B-A gauge-type ion gun, a gas introduction system, and an entry-lock system. It is evacuated by 150 l/s turbomolecular and Ti getter pumps, and the base pressure is 2×10^{-8} Pa. The RHEED gun is used as an excitation source in the AES measurement. The AES spectra were taken at the dI/dV mode with a lock-in amplifier (PAR Model 126) by applying 1 V of modulation on the sample. A primary electron energy of 15 keV was used in the RHEED and AES experiments.

Each single crystal of ZrB_2 (Refs. 8 and 9) and NbB_2 (Ref. 10) was grown by the rf-heated floating-zone method. The grown rod was oriented along the (0001) direction by

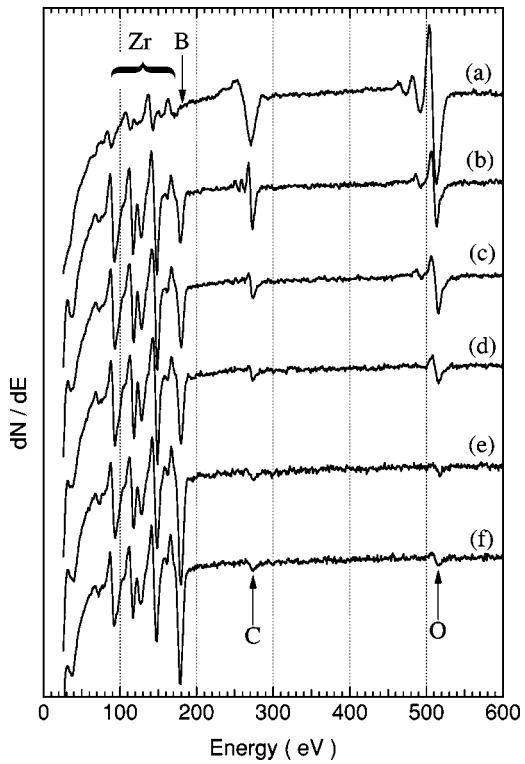

FIG. 1. AES spectral change in cleaning of $ZrB_2(0001)$. A polished sample (a) is heated at (b) 1400 °C, (c) 1570 °C, and (d) 1830 °C. Flash heating at (e) 1900 °C and (f) 2100 °C after repeated 1830 °C flashing produced an almost clean surface.

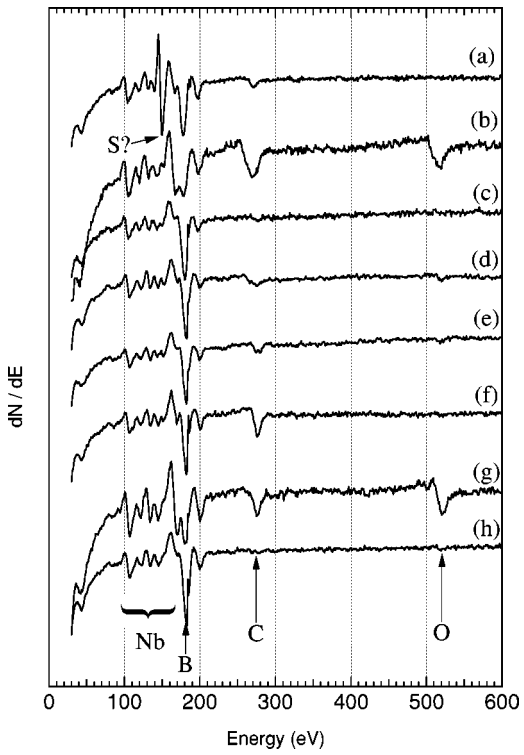

FIG. 2. AES spectra in cleaning of $NbB_2(0001)$. (a) is for the sample degassed at 1300 °C showing a 2×2 RHEED pattern. (b) Ion bombarded and (c) following annealed surfaces at 1300 °C. (d) CO is adsorbed from the residual gas, and (e) carbon remains after heating at 1300 °C, showing a weak $\sqrt{3}\times\sqrt{3}$ structure in RHEED. (f) Carbon is accumulated by the heating cycles and the $\sqrt{3}\times\sqrt{3}$ spots becomes clearer. (g) Ion bombardment and (h) annealing at 1300 °C recovers a clean surface.

using an x-ray Laue camera within the accuracy of 1°. Sample disks (6–8 mm in diameter and ~1 mm in thickness) were cut by a spark erosion method. One side of the sample was mechanically polished with diamond (9 μm in rough polishing and 3 μm in medium polishing) and alumina power (1 μm, final) to a mirror finish.

The sample was clipped on a small Ta frame by Ta strips or wires, and was introduced in the chamber. The sample can be heated in the vacuum by electron bombardment from the back side up to the temperature of 2000 °C. The sample temperature was measured by a two-color optical pyrometer with accuracy of a few tens of degrees.

III. RESULTS

A. Cleaning process

1. ZrB_2 (0001)

In the preparation chamber, the sample was at first heated up to 1000 °C for degassing. After waiting for the vacuum to recover, the sample was flash heated at 1400 °C–1570 °C several times. The AES spectral change is shown in Figs. 1(a)–1(c). In this sequence, the RHEED shows a diffuse 1×1 pattern. The surface was still contaminated by oxygen and carbon. Flash heating at 1830 °C twice results in a fairly sharp 2×2 RHEED pattern and reduction of the C and O contamination as shown in Fig. 1(d). This 2×2 surface may be the same as what was observed on the $HfB_2(0001)$.[11] After repeating the 1830 °C and finally 1900 °C flashing several times, the RHEED shows a sharp 1×1 pattern. The AES shows little contamination and growth of the B peak as shown in Fig. 1(e). The residual C and O is considered to be adsorbed during the measurement in a working pressure of $2-3\times10^{-7}$ Pa. Probably the surface structural change is related with the composition change at the surface. Neither the RHEED nor the AES changed further at higher flashing temperature [Fig. 1(f)]. This surface was measured as a clean 1×1 surface of $ZrB_2(0001)$ in the following.

The sample was transferred into the HREELS chamber in a vacuum. The sample azimuth was adjusted by LEED along $[11\bar{2}0](\bar{\Gamma}\text{-}\bar{K})$ or $[10\bar{1}0](\bar{\Gamma}\text{-}\bar{M})$. Just before starting each HREELS measurement, the sample was cleaned by flash heating at 1900 °C. It took typically 2–2.5 h to take an off-specular spectrum in a good S/N ratio. The vacuum (4×10^{-9} Pa) was good enough to keep the sample clean during the measurement.

2. NbB_2 (0001)

The degassed sample was flash heated at about 1300 °C several times. The RHEED pattern was a sharp 2×2 pattern and it showed an AES spectrum as in Fig. 2(a). Besides Nb (100–200 eV) and B (180 eV) Auger signals, there is a large

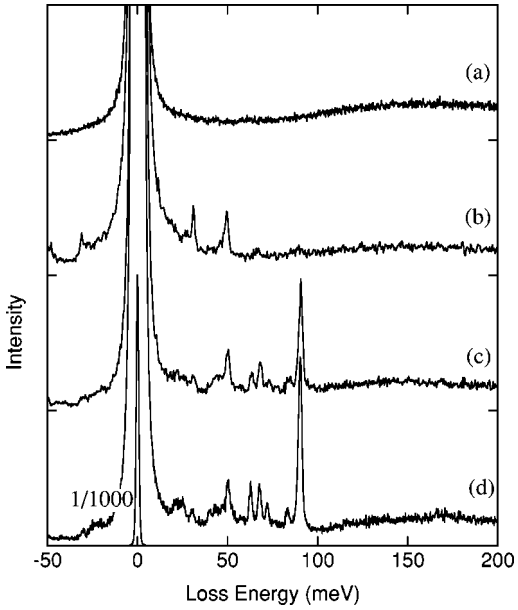

FIG. 3. Specular HREELS spectra for (a) clean $ZrB_2(0001)$ and (b) clean $NbB_2(0001)$. (c) and (d) show spectra for $NbB_2(0001)$ taken ~3 h and ~15 h after flashing, respectively. The primary electron energy E_0 is 32.3 eV. The sample azimuth is $[10\bar{1}0]$.

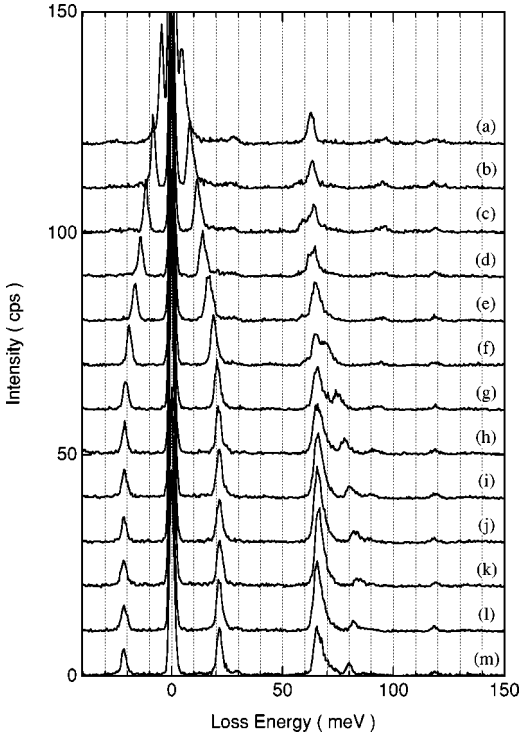

FIG. 4. A series of off-specular HREELS spectra for $ZrB_2(0001)$ along $[10\bar{1}0]$ $(\bar{\Gamma}-\bar{M})$. $E_0=32.3$ eV. The incidence angle θ_i is 75° from the surface normal. The detection angle θ_o is (a) 66.7°, (b) 61.0°, (c) 56.4°, (d) 53.0°, (e) 49.5°, (f) 46.1°, (g) 42.6°, (h) 40.3°, (i) 38.1°, (j) 35.8°, (k) 33.5°, (l) 31.2°, and (m) 28.9°.

peak at 150 eV and a small trace at 270 eV, which correspond probably to S and C contamination, respectively. In order to remove the contamination, Xe-ion bombardment was performed under the following conditions; ion energy =230 eV, ion current =0.6 μA, incidence angle ~60° from the surface normal, and Xe gas pressure $\sim 2\times10^{-3}$ Pa. After the bombardment, the RHEED pattern changed into a 1 $\times$1 with high background. In the AES spectrum as shown in Fig. 2(b), the 150 eV peak was removed while usual contaminants of C and O appeared. By annealing this surface to 1300 °C, a clean surface was obtained, in which no impurity was observed [Fig. 2(c)] and the RHEED showed a sharp 1 $\times$1 pattern. The intensity of Nb peaks versus B obviously decreased by the annealing after the ion bombardment [Figs. 2(b) and 2(c)]. This fact is consistent with B-layer termination of this surface.

When the clean surface is put in a vacuum of 4×10^{-7} Pa for a few tens of minutes, the residual gas CO is adsorbed on the surface as shown in Fig. 2(d). By flashing the surface, oxygen disappeared but carbon remained as shown in Figs. 2(e) and 2(f), resulting in a $\sqrt{3}\times\sqrt{3}$ structure. Probably, this structure corresponds to a commensurate overlayer of graphite. The appearance of the $\sqrt{3}\times\sqrt{3}$ structure was always accompanied by the carbon peak in the AES. Once the $\sqrt{3}\times\sqrt{3}$ structure is formed, it is difficult to recover the clean surface only by heating. The ion bombardment followed by the annealing can reproduce the clean surface [Figs. 2(g) and 2(h)]. In this experiment, the ion-bombarded sample was transferred to the HREELS chamber and annealed in the good vacuum to avoid the carbon accumulation. Before each HREELS measurement, the sample was flash heated at 1300 °C. It was confirmed that the surface kept the 1×1 structure after finishing all the measurements.

B. HREELS

The HREELS data were taken at three primary energies to observe the phonon modes having a different dependence of the cross section on the electron energy. The electron incidence angle θ_i was fixed at 75 ° from the surface normal and the detection angle θ_o was changed to scan the phonon wave vector.[12]

Figures 3(a) and 3(b) show specular spectra ($\theta_i=\theta_o$) for the clean $ZrB_2(0001)$ and the clean $NbB_2(0001)$, respectively. The specular spectrum for $ZrB_2(0001)$ shows no clear loss peak. As dipole-active modes are sensitively observed in the specular mode,[12] this result indicates that the surface is metallic enough to cover up the dipole field beneath. On the other hand, the specular spectrum for $NbB_2(0001)$ [Fig. 3(b)] shows clear loss peaks at 31.0 meV and at 49.4 meV, and small peaks at 66.5 meV and 89.1 meV. After a few hours, the 89.1 meV peak grows largely as shown in Figs. 3(c) and 3(d). Additionally, several new small loss peaks appear. These peaks correspond to the surface impurity vibration itself or the substrate mode that is emphasized by the impurity-induced charge. Anyway, the shielding effect on $NbB_2(0001)$ is not so complete compared with that on $ZrB_2(0001)$. This result is consistent with the surface termi-

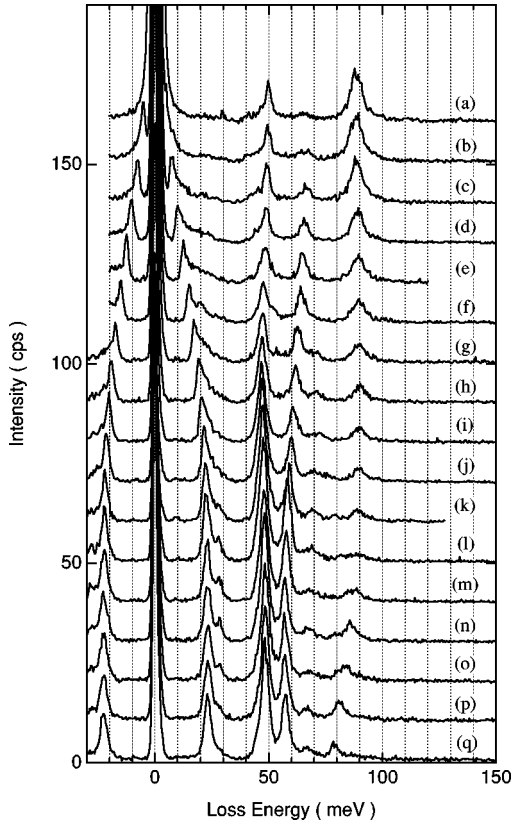

FIG. 5. A series of off-specular HREELS spectra for $NbB_2(0001)$ along $[10\bar{1}0]$ $(\bar{\Gamma}-\bar{M})$. $E_0=32.3$ eV. $\theta_i=75°$. θ_o = (a) 69.8°, (b) 65.7°, (c) 62.1°, (d) 58.9°, (e) 56.0°, (f) 53.2°, (g) 50.7°, (h) 48.3°, (i) 46.0°, (j) 43.7°, (k) 41.6°, (l) 39.5°, (m) 37.5°, (n) 35.6°, (o) 33.7°, (p) 31.8°, and (q) 29.9°.

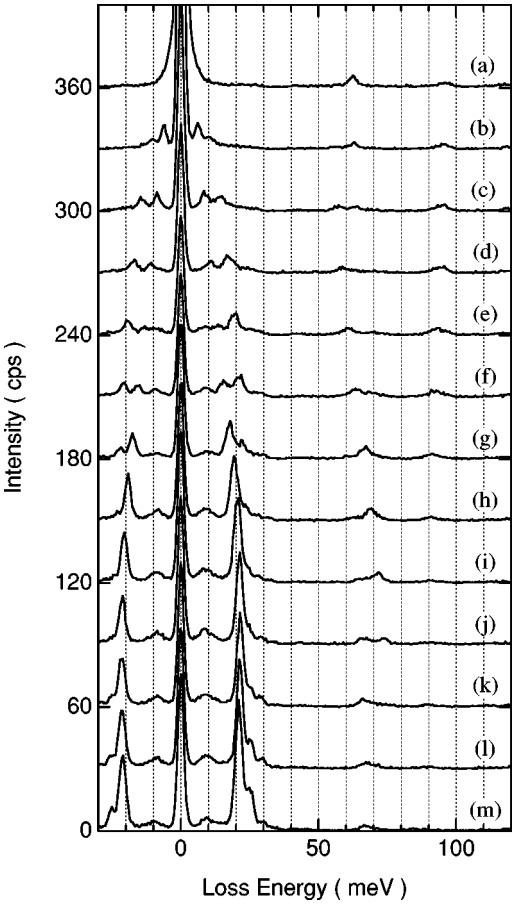

FIG. 6. A series of off-specular HREELS spectra for $ZrB_2(0001)$ along $[11\bar{2}0]$ $(\bar{\Gamma}-\bar{K})$. $E_0=22.4$ eV. $\theta_i=75°$. θ_o =(a) 68°, (b) 63°, (c) 58.5°, (d) 55°, (e) 51.5°, (f) 48°, (g) 45°, (h) 42°, (i) 39°, (j) 36.5°, (k) 34°, (l) 31.5°, and (m) 29°.

nation with metal atoms in $ZrB_2(0001)$ and with boron atoms in $NbB_2(0001)$, respectively.

Figures 4–7 show examples of series of off-specular spectra. One optical mode is resonantly strengthened on $NbB_2(0001)$ as shown in Figs. 7(i)–7(m), but not on $ZrB_2(0001)$ (Fig. 6) under the same conditions. In many spectra, the optical branches appear larger on $NbB_2(0001)$ than on $ZrB_2(0001)$, which seems consistent with the boron and metal termination of the respective surfaces. But in some cases, the intensity difference is small as shown in Figs. 4 and 5. In order to discuss further the peak intensity, dynamical calculations of low-energy electron diffraction will be necessary.[13]

The phonon dispersion determined from these data is plotted in Figs. 8 and 9. Energy of the phonon modes are divided into acoustic bands less than 30 meV and optical bands from 40 meV to 95 meV. The optical-phonon bands, to which the boron vibration mainly contributes, are clearly different between the two surfaces. On $NbB_2(0001)$, more branches are observed and the energy is lower than on $ZrB_2(0001)$. The model calculation discussed in the next section shows that the surface boron modes and the bulk boron modes are overlapped on the $NbB_2(0001)$. As the surface boron loses half bonds to adjacent metal atoms, the surface mode is fairly softened. On the other hand, the observed optical-phonon band on $ZrB_2(0001)$ corresponds to the boron phonon modes in the bulk.

IV. DISCUSSION

The observed phonon modes can be classified into two types: the acoustic modes (branches labeled a and b in Figs. 8 and 9) and the optical modes [Figs. 8(c)–8(h) and 9(c)–9(h)]. Considering the mass ratio of metal and boron atoms, the metal (boron) vibration mainly contributes to the former (latter) modes. In general, it is difficult to understand surface phonons without knowledge of bulk phonons. However, in the case of layered materials like graphite, the surface phonon dispersion is almost identical to the bulk one within the *c* plane because of the weak interlayer interaction. Although the interlayer (*M*-B) interaction is not so weak in MB_2 as in graphite, a large mass ratio between boron and metal atoms makes some phonon modes localized at the light (B) atoms. Namely, the interaction is small between B layers through the metal layer, because metal atoms with large mass isolate the B motion in that frequency region. Therefore, the B phonon modes are expected to have the character specific to layered materials. In this section, let us begin with a monolayer model to briefly interpret the boron phonon modes, followed by extending it to a multilayer slab model to examine the surface effect and the interlayer interaction effect.

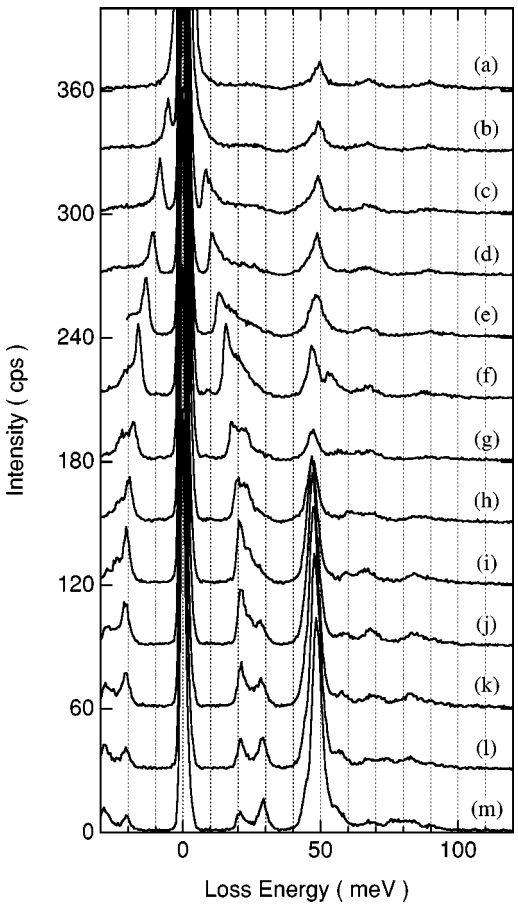

FIG. 7. A series of off-specular HREELS spectra for $NbB_2(0001)$ along $[11\bar{2}0]$ $(\bar{\Gamma}-\bar{K})$. $E_0=22.4$ eV. $\theta_i=75°$. θ_o = (a) 68°, (b) 63°, (c) 58.5°, (d) 55°, (e) 51.5°, (f) 48°, (g) 45°, (h) 42°, (i) 39°, (j) 36.5°, (k) 34°, (l) 31.5°, and (m) 29°.

A. Monolayer model

As the $NbB_2(0001)$ is considered to be boron terminated, which resembles the graphite monolayer (graphene) on a metal or metal-carbide substrate,[14–17] the phonon dispersion on this surface is analyzed by the monolayer model, which was useful in the graphene case. The observed boron phonon modes are assigned as follows on the analogy of the graphene case. The mode having the largest dispersion (branch e in Fig. 9) is assigned to the longitudinal-acousticlike (LA) mode, in which two boron atoms in a unit cell vibrate in phase. The mode that degenerates at the $\bar{K}$ point (branch f in Fig. 9) must be the longitudinal-optical (LO) mode. The other two modes (c and d in Fig. 9) which degenerate at the $\bar{K}$ point are the transverse modes having a displacement vector perpendicular to the surface. The lower-energy mode is an acousticlike mode (ZA) and the higher is an optical mode (ZO).

According to the graphene case,[15] a similar force-constant (FC) model is constructed. The model consists of a layer of honeycomb boron sheets adsorbed on a infinitely massive wall. In the boron layer, five FC's are adopted: the nearest-neighbor and the second-nearest-neighbor stretching FC's α_1 and α_2, the in-plane and out-of-plane nearest-neighbor angle bending FC's γ_1 and γ_2, and the bond twisting FC δ. In the graphene model, the stretching FC between the substrate and the overlayer in the perpendicular direction to the plane $\alpha_{s\perp}$ has been taken. The LA mode seemed to start at almost zero energy at the $\bar{\Gamma}$ point, indicating that the parallel component $\alpha_{s\parallel}$ is very small and has been neglected in the graphene case. Here the interaction between the overlayer and the substrate is stronger than in the graphene case and the parallel component is no longer negligible, because the LA mode has the finite value at the $\bar{\Gamma}$ point. The ratio between $\alpha_{s\perp}$ and $\alpha_{s\parallel}$ should be related to the B-Nb bond direction and unisotropy of the bond.

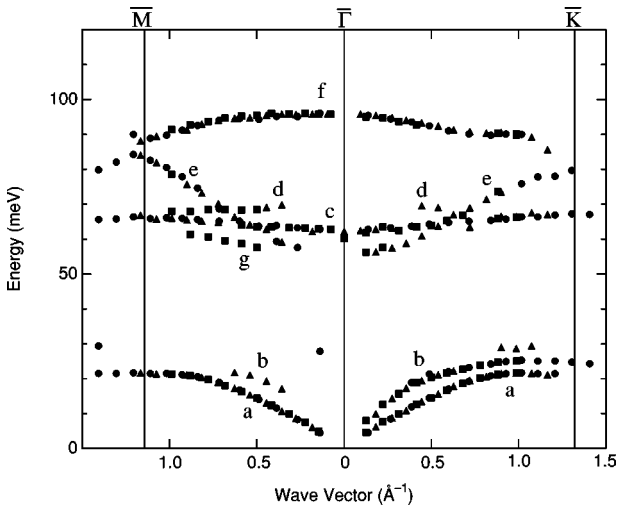

FIG. 8. Measured phonon dispersion for $ZrB_2(0001)$. Data points are taken from off-specular spectra for E_0 of 32.3 eV (circles), 22.4 eV (triangles), and 16.4 eV (squares).

Solid curves in Fig. 9 show the least-squares-fitted calculation result. The calculation generates six phonon modes because each unit cell contains two atoms. Within these six modes, two shear horizontal modes are not accessible by the electron-energy-loss spectroscopy according to the selection rule under the mirror symmetry.[12] The fitted parameters (FC's) are shown and compared with those for graphene on NbC(111) (Ref. 17) in Table I. The least-squares fitting indicates even negative values in δ and γ_1 although it is not clear whether these negative values are meaningful or not. Anyway, all intralayer FC's (α_1, α_2, γ_1, γ_2, and δ) on $NbB_2(0001)$ are clearly smaller than those on the graphene, corresponding to a larger interatomic distance in the boron layer. On the other hand, the interlayer FC α_s increases. In NbB_2, the bond strength between B atoms in the B layer is comparable to that between B and Nb. In a viewpoint of bonding nature, NbB_2 does not have a strong character as a layered material.

B. Slab model

As shown in Fig. 9, the monolayer model reproduces the data fairly well, but some observed boron modes remain unexplained (branches g and h in Fig. 9). These modes are probably derived from B layers in the bulk. The acoustic modes (a and b in Fig. 9) cannot be explained by the mono-

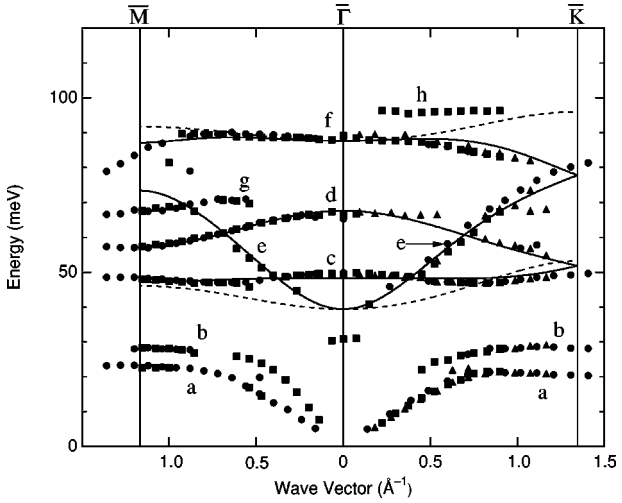

FIG. 9. Measured phonon dispersion for $NbB_2(0001)$. Data points are taken from off-specular spectra for E_0 of 32.3 eV (circles), 22.4 eV (triangles), and 14.4 eV (squares). Solid and dashed curves represents the calculation result of the monolayer model described in the text. Dashed lines correspond to shear horizontal modes which are not accessible by HREELS. The mode c is assigned to ZA, d to ZO, e to LA, and f to LO.

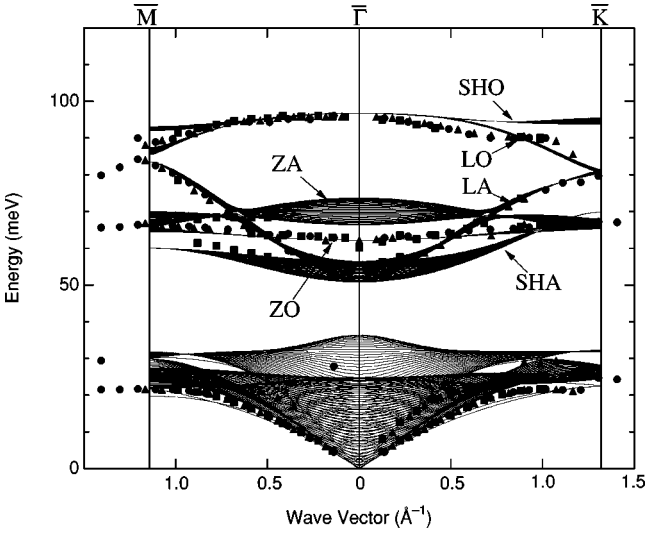

FIG. 10. Calculated phonon-dispersion curves for the 81-layer Zr-terminated slab model fitted to the ZrB_2 data. The same experimental data as in Fig. 8 are plotted again for comparisons.

layer model, either. The model must be improved to a more realistic multilayer version in order to give any solution to these problems. Here, a slab model which consists of 79 or 81 atomic layers is used. In place of the FC's $\alpha_{s\perp}$ and $\alpha_{s\parallel}$, a stretching FC α_3 and an correction parameter $\alpha_{3\parallel}$ are taken between adjacent metal and boron atoms. α_3 corresponds to the usual central force and $\alpha_{3\parallel}$ is the FC which works only along a plane parallel to the surface. The latter is necessary to adjust the ZA mode and the LA mode independently at the $\bar{\Gamma}$ point. This parameter may be indicative of unisotropy in the covalent bond between boron and metal atoms. Between metal atoms, an intralayer stretching FC α_4 and an interlayer *M*-*M* stretching FC α_5 are adopted.

At first, the parameters were tentatively set to the fitted values in the monolayer model and similar values in the pure metal crystal for α_4 and α_5. Calculated dispersion curves are compared with the experimental data and judged by the eye. The parameters are changed until the calculation reasonably matches the data. In order to reduce the number of the parameters, the twisting FC δ is omitted here.

TABLE I. Lattice-constant and fitted force-constant parameters for the monolayer model.

Parameter	$NbB_2(0001)$	Graphene on NbC(111)
a(nm)	0.311	0.252
α_1 (10^4dyn/cm)	8.80	33.9
α_2 (10^4dyn/cm)	1.32	4.96
γ_1 (10^{-12}erg)	−0.095	6.66
γ_2 (10^{-12}erg)	0.848	1.68
δ (10^{-12}erg)	−0.917	1.89
$\alpha_{s\perp}$ (10^4dyn/cm)	9.81	4.9
$\alpha_{s\parallel}$ (10^4dyn/cm)	6.65	

A slab consisting of 81 atomic layers (40 B layers and 41 Zr layers), both surfaces of which are terminated by the metal layer, was taken as a model for $ZrB_2(0001)$. Figure 10 shows the fitted calculation result with the experimental data. The obtained parameters are listed in Table II.

In Fig. 11, grey-scale maps of the phonon local density of states (LDOS) of the atom i in the wave vector parallel to the surface $\mathbf{k}$—the phonon energy E space $\rho_{\alpha i}(\mathbf{k},E)$ are shown. Here, $\rho_{\alpha i}(\mathbf{k},E)=\Sigma_j|v_{\alpha ij}|^2\delta(E-\hbar\omega_j))$; ω_j and $\mathbf{v}_{ij}$ are the jth eigenfrequency and eigenvector for the wave vector $\mathbf{k}$, respectively. α represents the Cartesian axis. The δ function is taken as a gaussian function having 1 meV full width at half maximum to simulate the phonon lifetime and the experimental resolution. It is confirmed that the high-energy modes are localized at the boron layers. The phonon dispersion of the second B layer [Figs. 11(c) and 11(d)] is almost same as that of the middle (the 41st in depth) B layer [Figs. 11(e) and 11(f)]. Considering the surface relaxation, the FC near the surface can be different from the bulk values. However, changing of the FC α_3 at the surface by about $\pm 10\%$ does not largely affect the second layer phonon dispersion.

TABLE II. Fitted force constants for the slab model.

Parameter	$ZrB_2(0001)$	$NbB_2(0001)$
a(nm)	0.317	0.311
c(nm)	0.353	0.329
α_1 (10^4dyn/cm)	7.4	8.8
α_2 (10^4dyn/cm)	0.8	1.3
γ_1 (10^{-12}erg)	1.1	0.0
γ_2 (10^{-12}erg)	−0.2	1.0
α_3 (10^4dyn/cm)	6.3	5.6
$\alpha_{3\parallel}$ (10^4dyn/cm)	0.3	0.4
α_4 (10^4dyn/cm)	2.5	2.0
α_5 (10^4dyn/cm)	2.5	1.5

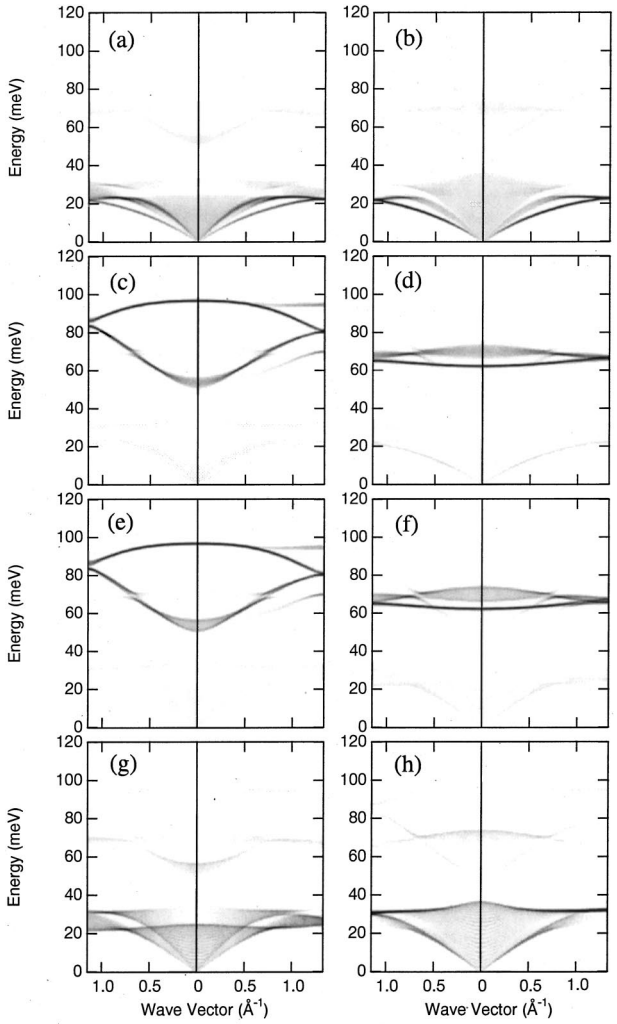

FIG. 11. Calculated phonon LDOS in the ZrB_2 slab model for (a) the first layer's longitudinal component, $\rho_{x,Zr(1)}$, (b) the first layer's transverse component perpendicular to the surface, $\rho_{z,Zr(1)}$, (c) the second layer's longitudinal, $\rho_{x,B(2)}$, (d) the second layer's z direction, $\rho_{z,B(2)}$, (e) the 40th layer's one, $\rho_{x,B(40)}$, (f) $\rho_{z,B(40)}$, (g) $\rho_{x,Zr(41)}$, and (h) $\rho_{z,Zr(41)}$.

As one set of the boron phonon is observed on $ZrB_2(0001)$, it must be that the bulk mode and the surface relaxation should not be so large.

It is worth noting that the ZA mode is energetically higher than the ZO mode in this assignment. Metal atoms have larger vibrational amplitude in the ZA mode than in the ZO mode at the $\bar{\Gamma}$ point, because the boron atoms vibrate in phase in the former mode. This causes larger dispersion in the bulk phonon along the c axis and the ZA mode broadening as shown in Fig. 11(d). Only the lower-energy branch is observed in the experiment, which should be assigned as the energetically sharp band: the ZO mode. The ZA mode's frequency can become higher than the ZO assuming a very small angle bending FC γ_2. As the energy difference between the ZA mode and the ZO mode is very small, a large negative value is not necessary for γ_2.

In the case of $NbB_2(0001)$, the energy difference between the ZO mode and the ZA mode is larger than that of ZrB_2. If

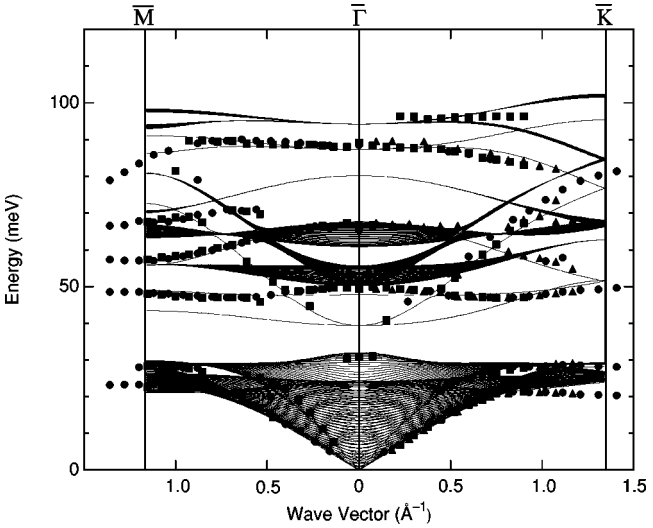

FIG. 12. Calculated phonon-dispersion curves for the 79-layer B-terminated slab model fitted to the NbB_2 data. The same experimental data as in Fig. 9 are plotted again for comparisons.

the high- (low-) energy mode were assigned to the ZA (ZO) mode, the angle bending FC (γ_2) would become largely negative, which is not probable. In fact, the loss peak intensity of the low-energy mode (~ 50 meV) is larger than the high-energy one (~ 67 meV) near the specular conditions as shown in Fig. 5 or in Fig. 3(b). This means the low-energy mode has larger dipole activity, which is consistent with the assignment above. As all boron atoms move together in the ZA mode, the dipole moment should be strengthened. In the ZO mode, the dipole field is compensated between adjacent boron atoms having opposite displacement.

Figure 12 shows the result for a 79-layer (40 B layers and 39 Nb layers) B-terminated slab fitted to the $NbB_2(0001)$ data. The parameters are shown in Table II. In this case, duplicate sets of dispersion curves having similar shapes appear at energetically different positions as shown in Fig. 13. One is the surface boron-layer modes in Fig. 13(a) and 13(b) appearing at lower energy, and the other is the bulk boron modes [Figs. 13(g) and 13(h)]. In general, the surface phonon of a layered material is similar to the bulk phonon because of the small interlayer interaction. In the NbB_2 case, the interlayer interaction is no longer small, causing the large softening of the surface phonon. The character of a layered material is read from the similar shape of the dispersion curves. The dispersion width perpendicular to the plane, which appears in Fig. 13(g) or 13(h) as the band broadening, is not so wide as in an isotropic crystal.

As the HREELS is surface sensitive, the main feature of the experimental data is assigned to the surface boron modes. The modes g and h in Fig. 9, which were not explained in the monolayer model, seem to correspond to the bulk boron modes in the slab model. Unfortunately, it is difficult to discuss quantitatively how the surface boron layer changes from the bulk one (surface relaxation), because the bulk modes are not completely observed in the experiment.

In a qualitative comparison between $ZrB_2(0001)$ and $NbB_2(0001)$, the following features can be read; (a) the

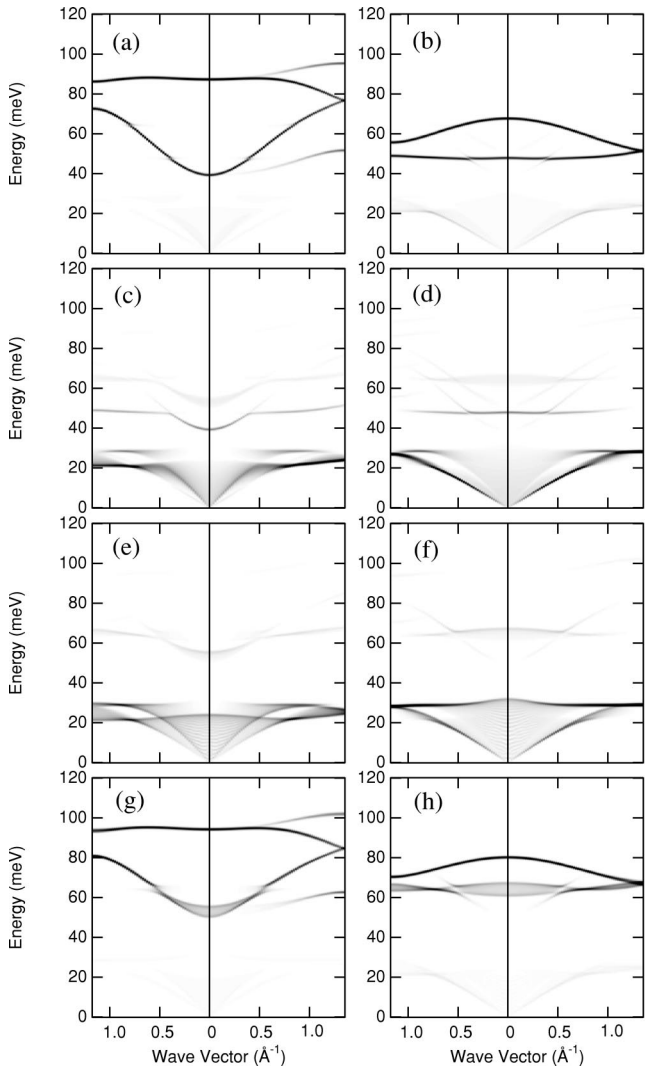

FIG. 13. Calculated phonon LDOS in the NbB_2 slab model. (a) $\rho_{x,B(1)}$, (b) $\rho_{z,B(1)}$, (c) $\rho_{x,Nb(2)}$, (d) $\rho_{z,Nb(2)}$, (e) $\rho_{x,Nb(40)}$, (f) $\rho_{z,Nb(40)}$, (g) $\rho_{x,B(41)}$, and (h) $\rho_{z,B(41)}$.

angle bending FC within the plane (γ_1) is largely reduced in NbB_2, (b) the out-of-plane bending FC (γ_2) is reduced in ZrB_2, (c) the B-B stretching FC's (α_1 and α_2) are smaller in ZrB_2 than in NbB_2, and (d) the B-*M* stretching FC's (α_3) are larger in ZrB_2. As the FC γ_2 is thought to be indicative of the π-bond strength in the boron sheet, feature (b) suggests that the π bond is stronger in NbB_2 than in ZrB_2. However, it is not clear whether this π-bond difference is caused by the electron number (Zr belongs to group IV and Nb to group V) or by the surface effect (the ZrB_2 data come from the bulk boron while the surface boron layer mainly contributes to the NbB_2 data). Further theoretical study or bulk phonon-dispersion data will be necessary to clarify this point. Feature (c) sounds consistent with the variation of lattice parameter *a*, while feature (d) seems inconsistent with the variation in *c*. Probably the small B-Nb stretching FC is caused by the surface relaxation. As main parts of the NbB_2 phonon data come from the surface boron layer, the obtained FC parameters reflect those in the surface layer. The ICISS experiment[4] revealed large outward relaxation (+8.5%) of the surface boron layer on $TaB_2(0001)$. If the surface boron layer is largely relaxed also on $NbB_2(0001)$, the small FC is consistently explained by the expansion of interlayer distance at the surface.

TABLE III. Nearest-neighbor bond length and stretching force constant in ZrB_2 and LaB_6.

	Bond length (nm)	Stretching FC (10^4 dyn/cm)
B-B bond		
ZrB_2 [a]	0.183	7.4
LaB_6 (nearest neighbor) [b]	0.167	17.3
LaB_6 (secondnearest neighbor) [b]	0.176	11.6
B-*M* bond		
ZrB_2 [a]	0.254	6.3
LaB_6 [b]	0.224	1.5

[a]This work.
[b]Reference 18.

In Table III, the bond length and the stretching FC of ZrB_2 are compared with those in LaB_6.[18] The B-B bond length is slightly larger in ZrB_2 and the stretching FC is reduced accordingly. On the other hand, the stretching FC between B and Zr is much larger though the bond length is larger. This indicates that a strong covalent bond is formed between Zr and B in ZrB_2, while a weak ionic bond exists between La and B in LaB_6.

As far as the acoustic modes are concerned, the agreement is reasonable although not perfect. The interlayer metal-metal distance *c* is comparable to that within the layer *a*. Therefore, in the acoustic region where the metal atoms mainly vibrate, the dispersion along the *c* axis is very large, as it is in isotropic materials. The observed acoustic surface phonon no longer has the character of a layered material and becomes a ''surface mode'' in its original meaning. In fact, the LDOS shows that the surface acoustic mode is localized at the metal layer in the vicinity of the surface [Figs. 11(a), 11(b), 13(c), and 13(d)]. For further discussions, bulk phonon-dispersion data for MB_2 would be necessary.

V. SUMMARY

Phonon-dispersion relations for $ZrB_2(0001)$ and $NbB_2(0001)$ clean surfaces are measured by HREELS. The phonon modes of the boron layer are assigned to be bulk boron modes on $ZrB_2(0001)$ and a complex of bulk and surface boron modes on $NbB_2(0001)$. The dispersion data are analyzed by force-constant models under monolayer and multilayered slab constructions. The obtained force constants show that the B-B bond strength is comparable to the B-*M* bond. Comparing ZrB_2 with NbB_2, the B-B bond, especially the π bond, seems stronger in NbB_2 than in ZrB_2.

[1] J. Nagamatsu, N. Nakagawa, T. Muranaka, Y. Zenitani, and J. Akimitsu, Nature (London) **410**, 63 (2001).
[2] S.L. Bud'ko, G. Lapertot, C. Petrovic, C.E. Cunningham, N. Anderson, and P.C. Canfield, Phys. Rev. Lett. **86**, 1877 (2001).
[3] W. Hayami, R. Souda, T. Aizawa, and T. Tanaka, Surf. Sci. **415**, 433 (1998).
[4] H. Kawanowa, R. Souda, S. Otani, and Y. Gotoh, Phys. Rev. Lett. **81**, 2264 (1998).
[5] K. Yamamoto, K. Kobayashi, H. Kawanowa, and R. Souda, Phys. Rev. B **60**, 15 617 (1999).
[6] G. Benedek, F. Hofmann, P. Ruggerone, G. Onida, and L. Miglio, Surf. Sci. Rep. **20**, 1 (1994).
[7] H. Ibach, *Electron Energy Loss Spectrometers* (Springer, Berlin, 1991).
[8] S. Otani and Y. Ishizawa, J. Cryst. Growth **165**, 319 (1996).
[9] S. Otani, M.M. Korsukova, and T. Mitsuhashi, J. Cryst. Growth **186**, 582 (1998).
[10] S. Otani, M.M. Korsukova, and T. Mitsuhashi, J. Cryst. Growth **194**, 430 (1998).
[11] C.L. Perkins, R. Singh, M. Trenary, T. Tanaka, and Yu. Paderno, Surf. Sci. **470**, 215 (2001).
[12] H. Ibach and D. L. Mills, *Electron Energy Loss Spectroscopy and Surface Vibrations* (Academic Press, New York, 1982).
[13] D. L. Mills, S. Y. Tong, and J. E. Black, *Surface Phonons*, Springer Series in Surface Science, Vol. 21, edited by W. Kress and F. W. de Wette (Springer-Verlag, Berlin, 1991), p. 193.
[14] T. Aizawa, R. Souda, S. Otani, Y. Ishizawa, and C. Oshima, Phys. Rev. Lett. **64**, 768 (1990).
[15] T. Aizawa, R. Souda, S. Otani, Y. Ishizawa, and C. Oshima, Phys. Rev. B **42**, 11 469 (1990); **43**, 12 060 (1991).
[16] T. Aizawa, R. Souda, Y. Ishizawa, H. Hirano, T. Yamada, K. Tanaka, and C. Oshima, Surf. Sci. **237**, 194 (1990).
[17] T. Aizawa, Y. Hwang, W. Hayami, R. Souda, S. Otani, and Y. Ishizawa, Surf. Sci. **260**, 311 (1992).
[18] K. Takegahara and T. Kasuya, Solid State Commun. **53**, 21 (1985).